The DED at TEXTOR: transport and topological properties of a helical divertor

M. Lehnen[1)], S. Abdullaev[1)], S. Brezinsek[1)], M. Clever[1)], J.W. Coenen[1)], K.H. Finken[1)], M. von Hellermann[2)], M.W. Jakubowski[3)], D. Reiter[1)], U. Samm[1)], D. Schega[1)], O. Schmitz[1)], H. Stoschus[1)], B. Unterberg[1)] and the TEXTOR team

[1)] *Institut für Plasmaphysik, Forschungszentrum Jülich GmbH, EURATOM Association, Trilateral Euregio Cluster, D-52425 Jülich, Germany*

[2)] *FOM-Institute for Plasma Physics Rijnhuizen, Association EURATOM-FOM, Trilateral Euregio Cluster, The Netherlands, www.rijnh.nl*

[3)] *Max-Planck-Institut für Plasmaphysik, IPP-EURATOM Association, Teilinstitut Greifswald, Wendelsteinstr. 1, 17491 Greifswald, Germany*

The topological and transport properties in the edge plasma of the dynamic ergodic divertor is studied to clarify the functionality of this type of helical divertor. The heat and particle fluxes at the DED target plates were measured with Langmuir probes. Peak fluxes are found where field lines end, which penetrate deep into the plasma. The comparison of the measured target profiles to the magnetic topology shows, that heat and particles are mainly transported to the target plates via flux tubes of short connection length. About 65% of the fluxes are found in areas, where field lines with a connection length of 1-2 poloidal turns connect to the target. Analysis of the source distribution shows, that about 40% of the ion sources lie inside the downstream area of the divertor. The high fraction of convective heat flux prevents from establishing high recycling in the divertor for the pulse type discussed here.

Keywords: TEXTOR, stochastic plasmas, divertor

Introduction

The aim of this paper is to quantify the particle and power exhaust capabilities of the dynamic ergodic divertor (DED) at TEXTOR. The DED is a helical type of divertor with an open structure, comparable to the ergodic divertor in ToreSupra [1] . Such a divertor has topological similarities to helical or island divertors in heliotrons [2] or stellarators [3]. The ergodic divertor, existing of 16 helical coils at the HFS of TEXTOR, generates a resonant magnetic perturbation which focuses the particle and heat flux onto divertor target plates. In contrast to a poloidal divertor with a clear boundary between scrape-off layer and confined plasma, the above mentioned divertor types have a region with magnetic islands in the edge layer. By island overlap, this area turns (partly) into an ergodic layer.

Topology

The magnetic topology of the DED is determined by the position of the resonant surfaces (surfaces with low rational safety factor) and the base mode of the divertor coil current distribution [4]. Three base modes can be chosen with poloidal/toroidal mode numbers of $m/n = 3/1, 6/2$ and $12/4$. The spectrum of the $m/n = 6/2$ perturbation field is given in figure 1. Depending on the base mode, 2, 4 or 8 helical strike zones appear on the divertor target. An example of the target footprint for $m/n = 6/2$ is given in figure 2. The colors indicate the penetration depth of the field lines. Peak particle and heat fluxes are found where field lines of long connection length hit the target. This is caused by the deep penetration of these field lines up to the last closed flux surface (LCFS). Flux tubes of one poloidal turn length are positioned further away from the LCFS [5, 6, 7]. They are filled by diffusion and can take a substantial part of the particle and heat to the target. The target structure is sensitive to the plasma equilibrium,

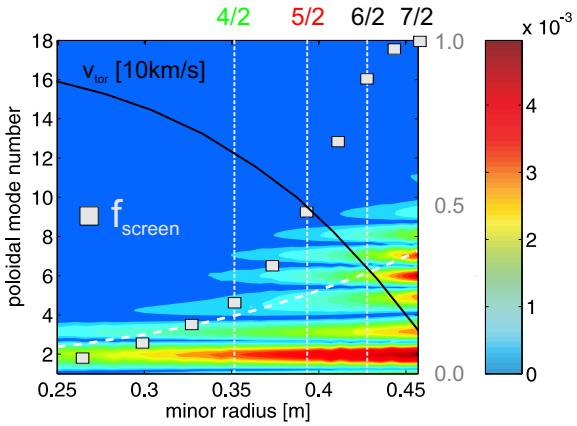

Fig. 1 *Spectrum of the perturbation field B_{m2} [T] for $m/n = 6/2$. The white dashed line indicates the position of the resonances. The gray rectangles give the screening factor for a typical edge rotation.*

author's e-mail: m.lehnen@fz-juelich.de

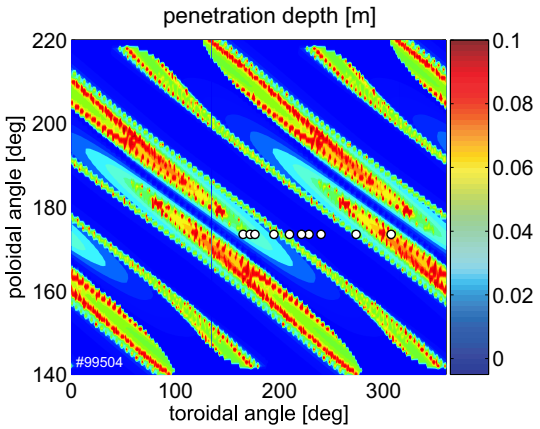

Fig. 2 *Map of the penetration depth of field lines starting on the DED target. The white circles indicate the position of the target Langmuir probes.*

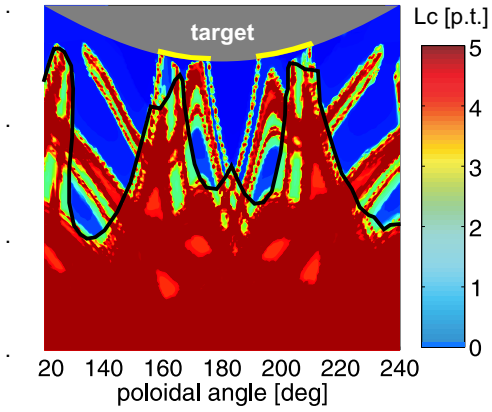

Fig. 3 *Connection length of the field lines passing the poloidal plane in front of the target at $\phi = 180°$. The strike lines are indicated in yellow. The black line indicates the boundary of the downstream area.*

e.g. edge safety factor, plasma beta and plasma position. Moreover, plasma rotation can lead to screening currents, reducing the perturbation at the resonances [8, 9]. An example for a screening factor is indicated in figure 1; the toroidal rotation increases from about 1 km/s at the LCFS up to 10 km/s in the plasma center. The screening is relatively weak at the very edge, because of low plasma rotation and low temperature. Towards the plasma center, the screening increases. Thus the magnetic topology calculated usually for the vacuum case is valid for the outermost resonance layers. However, further inside, the size of the islands shrinks with higher plasma rotation and the width of the ergodic area is affected. In the following we concentrate on a pulse with $m/n = 6/2$, $q_a = 3.6$, $\beta \approx 0.45$ and the horizontal position off-center by $2 - 5$ cm towards the HFS to ensure particle recycling only at the divertor target plates.

A poloidal cut through the magnetic structure at $\phi = 180°$ is given in figure 3 for full perturbation field. This plot shows the connection length of the field lines from target to target as a function of poloidal angle and radius. A strong intermixture between field line bundles of long and short connection length exists. The particles and heat are guided to the target along complex structures of about 15 cm width in poloidal direction, when touching the target. It is remarkable, that the wetted area is mainly defined by the topology rather than by transport properties (c.f. [10]). The field line bundles with short connection length of less than 5 poloidal turns constitute the so called laminar area of about 7 cm width in this example. The link between last closed flux surface (LCFS) and this laminar region is the ergodic area of about 4 cm width.

Target Loads

Figure 4 shows the particle and heat flux at the target measured by Langmuir probes which are indicated in figure 2. A full profile is achieved by sweeping the strike point by ±22.5° in toroidal direction. This is possible with a coil current of 3.75 kA, which is half of the nominal coil current. The discharge had a total heating power of 1.1 MW and a radiated power of 0.5 MW, thus the power entering the edge layer P_{edge} is about 0.6 MW. The wetted area is, for the case shown here, $A = 2.4\text{m}^2$. The radial decay of heat and particle flux is mapped on the poloidal coordinate on the target with an expansion of about 2. From the probe measurements, we get an average parallel heat flux of about 20MWm^{-2} in the strike point, which is consistent with a perpendicular heat flux of $P_{edge}/A \approx 0.3\text{MWm}^{-2}$, taking into account an average pitch angle of about 0.8° at the target. Because of the very shallow angle, slight misalignment of the target tiles leads to a non-regular distribution of the heat along the strike points in toroidal direction as seen by the infra-red camera [11]. However, the probes stick out by 2 mm (dome probe with $r = 2$ mm) and are therefore less sensitive to flux shadowing.

Additionally to the fluxes, the connection length L_c and also the penetration depth Δr of the field lines is indicated in figure 4. The calculation was done by field line mapping. To fit the target profiles best, a slight deviation from the experimental settings had to be chosen: a 5 kA higher plasma current (less than 2% higher than the measured current) and a 6° shift in toroidal direction. With this, the best fit of the strike point separation and toroidal position is achieved. Such adaptations are justified, taking into account the measurement errors on the discharge parameter and the uncertainties in the safety factor profile assumed for the field line mapping. Additionally, the probe has a radial extent of 2 mm, giving an uncertainty in toroidal direction of about 10 cm.

The area with $L_c < 1$ poloidal turn (p.t.) is equivalent to the private flux region. In this area almost no flux is reaching the divertor. About 65% of the particle and heat flux is transported to the target plates via flux tubes with 1 or 2 poloidal turns ($L_c = 40 - 80$ m). The magnitude of the

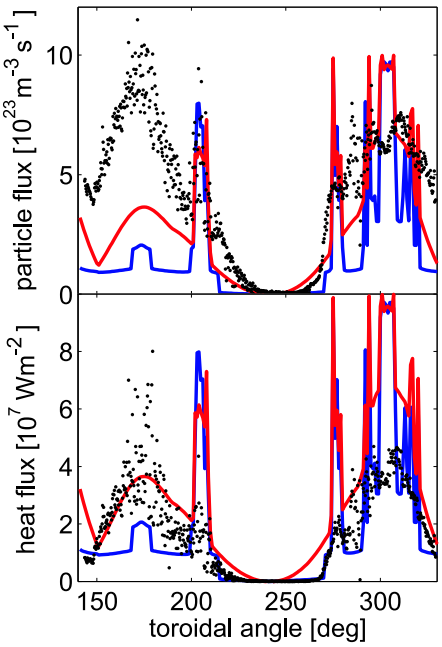

Fig. 4 *Particle flux on the target along the toroidal direction. The red curve gives the field line penetration depth in [10^{-2}m] (right axis) and the blue curve the connection length from target to target in poloidal turns (right axis).*

heat and particle flux depends on the penetration depth of the field lines with peak fluxes at field lines with deep radial penetration (c.f. [12, 13]). Those field lines are closest to the LCFS. The thickness of the perturbed edge layer and thus the maximum Δr is about 11 cm. The field lines with short connection length penetrate about 4 cm towards the LCFS. Only after many poloidal turns the field lines reach the innermost ergodised island chain and are thus close to the LCFS. However, the peak flux at the target for these field lines is not larger than that of the laminar field lines.

The information of the field line penetration in addition to the toroidal profiles of the fluxes can be used to reconstruct radial profiles of parallel heat and particle flux. The increase of the fluxes with Δr is shown in figure 5. Flux in the private flux region (L_c < 8m) is indicated in blue, flux in the laminar field line bundles with L_c = 40 − 80m are given in red and green are the data points for L_c > 2p.t.. From these profiles, e-folding lengths can be estimated. For this analysis the toroidal range with $\phi < 250°$ was chosen, because of the large fraction of short flux tubes. The e-folding lengths in the PFR is small, because of the short connection length: $\lambda_\Gamma = 3.5 \pm 0.4$ mm and $\lambda_q = 2.4 \pm 0.2$ mm for particle and heat flux. In the laminar flux bundles, these values are significant higher: $\lambda_\Gamma = (28 \pm 4)$ mm and $\lambda_q = (16 \pm 2)$ mm. The ratio between the e-folding lengths of PFR and flux tubes corresponds to the ratio of the connection lengths. Furthermore, the e-folding length of the electron density and temperature can be estimated to be $\lambda_T = 38 \pm 18$ mm and $\lambda_n = 45 \pm 23$ mm. Exploiting the relation between λ_n/λ_T and χ/D [14],

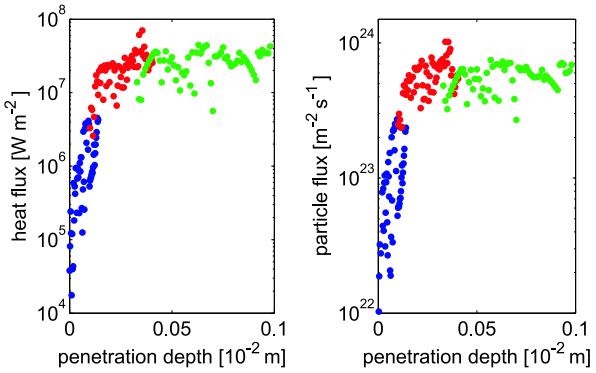

Fig. 5 *Particle and heat flux as function of the radial field line penetration.*

$$\frac{\gamma_e}{1 - f_{conv}} = \left(1 + \frac{\lambda_n}{\lambda_T}\right)\left(\frac{5}{2} + \frac{\chi}{D}\frac{\lambda_n}{\lambda_T}\right), \qquad (1)$$

we can estimate the fraction of convective heat flux f_{conv} to be about 0.6 (assuming $\chi/D = 3$).

Particle Recycling

The DED is an open divertor and the recycling neutrals can penetrate deep into the edge plasma by by-passing the high temperature and high density areas. However, in comparison to the helical divertor in an heliotron device like LHD [2], the divertor legs are broad and their radial extent is much smaller. Important for a high recycling divertor and for impurity screening is the closure of the divertor by localised recycling in the divertor chamber. The transition from divertor chamber to ergodic area in the DED can not be attributed to a distinct radial position. This can be seen from figure 3, giving the connection length of field lines in front of the DED target at a toroidal angle of 180°. One finds a complex mixture of different types of field lines. Field lines with long connection length can come close to the target plates, but connect to these only after they passed again several times the divertor coils (red areas). Thus, neutrals can penetrate into these flux bundles at an upstream position. The downstream area of the divertor comprises all field lines connecting within less than one poloidal turn to the target. This definition is equivalent to that of a poloidal divertor. This downstream area is indicated by the black line in figure 3.

The radial extent of the downstream area in the 6/2 base mode is at maximum 7 cm and varies, depending on the DED current and the edge safety factor. Local divertor recycling is established, when all the particle sources are located in the downstream region. A parameter reflecting the divertor recycling fraction is the ration between downstream sources Q_{down} and total source Q_{tot}, which equals the incoming flux, if no wall retention is assumed. In the experiment, Q_{down} is measured as the H_{alpha} line emission integrated over the downstream area and Q_{tot} is the total emission in front of the target. The distribution of the H_α

emission is shown in figure 6, together with a contour plot of the shortest connection length to the target. Field lines, which have to pass the divertor target again before they end on the target plates, belong to the upstream area. Sources in these field lines contribute to convective flux to the divertor.

The ratio between downstream D^+ sources and total D^+ source strength, Q_{down}/Q_{tot}, reaches values of up to 50% [15]. The fraction of the sources in the downstream area of the flux tubes with $1-2$ p.t. is about 25%. Assuming that $Q_{tot} = \Gamma_{tot}$, we get for these flux tubes $Q^{1,2}_{down}/\Gamma^{1,2} = 0.4$. Thus about 60% of the heat flux is transported convectively to the target in these flux tubes. Keeping in mind, that these are rough estimates, we find a good agreement with the above estimate from the e-folding lengths.

The accessibility of a high recycling regime can be assessed by including the convective heat flux into the two-point model:

$$q_{\|} = -\kappa_0 T^{5/2}\frac{\partial T}{\partial x} + (\frac{1}{2}mv_{\|}^2 + 5eT)\Gamma_{\|}\ . \qquad (2)$$

Neglecting the kinetic term and assuming that

$$\frac{\partial}{\partial x}\Gamma_{\|} = f_{conv}\frac{\Gamma_0}{L_c}\ , \qquad (3)$$

the heat flux equation $\partial q_{\|}/\partial x = q_{\|,t}/L_c$ can be solved. Figure 7 shows the temperature drop towards the target as function of the particle flux to the target. For the conditions of the pulse type discussed here ($f_{conv} = 0.6$ and $q_{peak} = 30\mathrm{MWm}^{-2}$), no temperature gradient can build up. Would a high recycling DED for this configuration be possible? Because of the density limit, the particle flux can not exceed $10^{24}\mathrm{m}^{-2}\mathrm{s}^{-1}$ significantly. Thus the access to high recycling needs a reduction of convective heat flux as well as a reduction of the power entering the edge layer. The latter could be achieved for example by higher radiation through impurity seeding. The absence of a high recycling regime has also be found in the helical divertor and in the island divertor. In the former case, because of the same reasons found for the DED, too high convective fluxes [16], and in the latter case, because of the significant role of the cross field transport inside the island [17].

Conclusions

The heat and particle fluxes at the DED target plates were measured with Langmuir probes. Peak fluxes are found where field lines end, which penetrate deep into the plasma. The comparison of the measured target profiles to the magnetic topology shows, that heat and particles are mainly transported to the target plates via flux tubes of short connection length. About 65% of the fluxes are found in areas, where field lines with a connection length of 1-2 poloidal turns connect to the target. Analysis of the source distribution shows, that about 40% of the ion sources lie inside the downstream area of the divertor. The high fraction of convective heat flux prevents from establishing high recycling in the divertor for the pulse type discussed here.

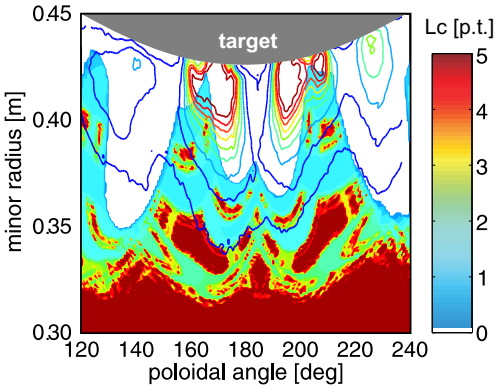

Fig. 6 *Magnetic structure in front of the DED target: shortest connection length to the divertor target. The contour lines indicate the intensity of the* H_α *radiation.*

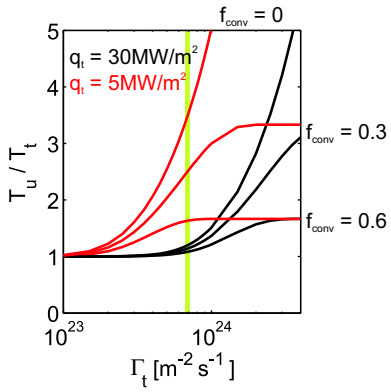

Fig. 7 *Temperature ratio between target und upstream position as function of the target particle flux. The green line indicates the peak particle flux for pulse #99504.*

[1] Ph. Ghendrih et al, Nucl. Fusion **42** (2002) 1221.
[2] T. Morisaki et al., J. Nucl. Mater. **337-339** (2005) 154
[3] R. König et al., Plasma Phys. Control. Fusion **44** (2002) 2365
[4] K.H. Finken et al., The structure of magnetic field in the TEXTOR-DED, Schriften des Forschungszentrum Jülich, Energy Technology **45**, ISSN 1433-5522 (2005)
[5] Th. Eich, D. Reiser and K.H. Finken, J. Nucl. Mater. **290-293** (2001) 849
[6] M. Lehnen et al. , Plasma Phys. Control. Fusion **47** (2005) B237
[7] O. Schmitz et al., J. Nucl. Mater. **363-365** (2007) 680
[8] A. Cole and R. Fitzpatrick, Phys. Plasmas **13** (2006) 032503
[9] Parail V. et al, Proc. 21st Int. Conf. Fusion Energy 2006 (Chengdu) (Vienna: IAEA) CD-ROM TP/P8-5
[10] S. Masuzaki et al., Nucl. Fusion **42** (2002) 750
[11] M.W. Jakubowski et al., J. Nucl. Mater. **337-339** (2004) 176
[12] M.W. Jakubowski et al., Plasma Phys. Control. Fusion **49** (2007) S109
[13] F. Nguyen et al., Nucl. Fusion **37** (1997) 743
[14] M. Lehnen et al., Nucl. Fusion 43 (2003) 168178
[15] M. Lehnen et al., J. Nucl. Mater. **363-365** (2007) 377
[16] M. Kobayashi et al., J. Nucl. Mater. **363-365** (2007) 294
[17] Y. Feng et al., Nucl. Fusion **46** (2006) 807